Biogeosciences Discuss., 7, 5047–5079, 2010
www.biogeosciences-discuss.net/7/5047/2010/
doi:10.5194/bgd-7-5047-2010

Biogeosciences Discussions

The most oligotrophic subtropical zones of the global ocean: similarities and differences in terms of chlorophyll and yellow substance

A. Morel, H. Claustre, and B. Gentili

Laboratoire d'Océanographie de Villefranche, Université Pierre et Marie Curie (Paris-6) and CNRS/INSU, UMR 7093, 06238 Villefranche-sur-mer, CEDEX, France

Received: 17 June 2010 – Accepted: 18 June 2010 – Published: 1 July 2010

Correspondence to: A. Morel (morel@obs-vlfr.fr)

Published by Copernicus Publications on behalf of the European Geosciences Union.

Abstract

The cores of the subtropical anticyclonic gyres are characterized by their oligotrophic status and minimal chlorophyll concentration, compared to that of the whole ocean. These zones are unambiguously detected by space borne ocean color sensors thanks to their typical spectral reflectance, which is that of extremely clear and deep blue waters. Not only the low chlorophyll (denoted [Chl]) level, but also a reduced amount of colored dissolved organic matter (CDOM or "yellow substance") account for this clarity. The oligotrophic waters of the North and South Pacific gyres, the North and South Atlantic gyres, and the South Indian gyre have been comparatively studied with respect to both [Chl] and CDOM contents, by using 10-year data (1998–2007) of the Sea-viewing Wide field-of-view Sensor (SeaWiFS, NASA). Albeit similar these oligotrophic zones are not identical regarding their [Chl] and CDOM contents, as well as their seasonal cycles. According to the zone, the averaged [Chl] value varies from 0.026 to 0.059 mg m^{-3}, whereas the $a_y(443)$ average (the absorption coefficient due to CDOM at 443 nm) is comprised between 0.0033 and 0.0072 m^{-1}. The CDOM-to-[Chl] relative proportions also differ between the zones. The clearest waters, corresponding to the lowest [Chl] and CDOM concentrations, are found near Easter Island and near Mariana Islands in the western part of the North Pacific Ocean. In spite of its low [Chl], the Sargasso Sea presents the highest CDOM content amongst the six zones studied. Except in the North Pacific gyre (near Mariana and south of Hawaii islands), a conspicuous seasonality appears to be the rule in the other 4 gyres and affects both [Chl] and CDOM; both quantities vary in a ratio of about 2 (maximum-to-minimum). Coinciding [Chl] and CDOM peaks occur just after the local winter solstice, which is also the period of the maximal mixed layer depth in these latitudes. It is hypothesized that the vertical transport of unbleached CDOM from the subthermocline layers is the main process enhancing the CDOM concentration within the upper layer in winter. In summer, the CDOM experiences its minimum which is delayed with respect to the [Chl] minimum; apparently, the solar photo-bleaching of CDOM is a slower process than the post-bloom

BGD
7, 5047–5079, 2010

algal Chl decay. Where they exist, the seasonal cycles are repeated without notable change from year to year; long term (10 years) trends have not been detected in these zones. These oligotrophic gyres can conveniently be used for in-flight calibration and comparison of ocean color sensors, provided that their marked seasonal variations are accounted for.

1 Introduction

Waters, extremely transparent to visible and near ultraviolet solar radiation, were found in the vicinity of Easter Island within the South Pacific anticyclonic gyre during the BIOSOPE cruise (Biogeochemistry and Optics SOuthPacific Experiment; Claustre et al., 2008). The hyperoligotrophic waters of this gyre are perhaps the "clearest" natural waters in the world ocean (Morel et al., 2007a,b). Such an extreme clarity primarily results from the very low level of the phytoplanktonic biomass; indeed, the chlorophyll concentration determined in the upper layer was below 0.03 mg m^{-3} (in November 2004; see Ras et al., 2008). The exceptional transparency within this oceanic water body also originates from the extremely low level of chromophoric dissolved organic material, CDOM (or "yellow substance", or "Gelbstoff"), as attested by the particularly low values of the attenuation coefficient for downward irradiance in the ultraviolet spectral domain (ibid., and Swan et al., 2009), and also attested by direct determinations (Bricaud et al., 2010). The special clarity of these waters results in a deep blue color due to the reflectance enhancement in the blue, violet, and UV parts of the spectrum. Space borne Ocean Color sensors are able to detect this enhancement. The recurrent detection from space of a huge "blue hole" denoting a hyperoligotrophic system within the South Pacific gyre is largely at the origin of the BIOSOPE project (Claustre and Maritorena, 2003).

Of course, the question arises about the possible occurrence of similar situations in other parts of the world ocean, not only in terms of algal concentration, but also in terms of yellow substance content. Other subtropical gyres also characterized by

BGD
7, 5047–5079, 2010

anticyclonic circulation, downwelling, and thicker thermoclines, are obvious candidates, since the depressed nutricline limits the algal development and subsequent biological/biochemical processes. These extensive oligotrophic gyres are well known in both hemispheres within the subtropical Atlantic and Pacific oceans. The south Indian ocean is also the seat of a subtropical anticyclonic system, while in the northern Indian ocean the monsoon regime impedes the regular development of such a similar feature. These desert oceanic areas have unambiguously been detected by ocean color sensors; their huge extension, and their chlorophyll concentration have been documented and monitored (see e.g., McClain et al., 2004; Polovina et al., 2008). Indeed, while the biological activity is comparatively small in these areas, their vast size makes their contribution to the global productivity and biogeochemistry definitely significant (see e.g., Antoine et al., 1996).

These ultramarine oceanic zones were also selected as offering wide and homogeneous targets allowing in-flight calibration of space ocean color sensors to be performed via the Rayleigh scattering calibration method (Fougnie et al., 2002). In this previous study, based on Sea-viewing Wide Field-of-view Sensor (SeaWiFS) data, the low chlorophyll level (thereafter denoted [Chl]) within several gyres has been confirmed and documented. No attempt, however, was made to comparatively assess the CDOM content. Yet, some years later, actually when the "GSM" algorithm (Siegel et al., 2002, 2005b) was applied to remotely sensed ocean color data, relative minima in near-surface CDOM abundance were also detected in the subtropical gyres. Therefore, a systematic study of these zones, with both their low [Chl] and low CDOM levels, can provide an answer to the initial question: do exist in the world ocean situations identical to, or approaching that one encountered near Easter Island from an optical viewpoint? More generally, and from a biogeochemical viewpoint, the trophic status of these zones, their seasonality, their systematic difference or resemblance, and the interannual stability of their characteristics are also the topics of the present study.

A newly proposed technique allows the chromophoric organic material content to be quantified from remotely sensed data of ocean color (Morel and Gentili, 2009a). This

BGD
7, 5047–5079, 2010

technique will be applied in parallel with the [Chl] retrieval to carry out a comparative study of the various oligotrophic subtropical gyres. The location and extension of the selected zones inside each of the gyres (Table 1 and Fig. 1) were delimited in order to contain the most oligotrophic inner core. Note that these zones are by far less extended than the ecological domains as defined in the sub-tropical regions by Longhurst (1995), or than the entire gyres as studied by McClain et al. (2004).

2 Data and methods

Satellite imagery (SeaWiFS) over the 1998–2007 period is considered for the present study. Yearly, monthly or eight-day L3 composites (9 km) of the [Chl] distribution, the PAR(0) distribution (the daily Photosynthetically Available Radiation at the surface), and distribution of the CDOM index (chromophoric dissolved organic matter) were used; they are the last values produced through the most recent NASA reprocessing (2009.1). The CDOM index is exactly the factor, which was defined and studied in Morel and Gentili (2009a), and denoted Φ. The meaning of this Φ index can be summarized as follows. In case 1 waters, there exists a "mean" relationship between the CDOM content and the chlorophyll concentration [Chl] (Morel, 2009) of the form

$$a_y(\lambda) = \alpha(\lambda)[\mathrm{Chl}]^{0.63},$$

where the CDOM content is expressed as an absorption coefficient (unit m^{-1}) at a certain wavelength, $a_y(\lambda)$. At the wavelength λ=443 nm for instance, the α coefficient amounts to 0.0316. Natural variability around the mean $a_y \leftrightarrow$[Chl] relationship is rather large; it is conveniently represented by introducing the index Φ (dimensionless) which modulates the mean relationship according to

$$a_y(443) = 0.0316\Phi[\mathrm{Chl}]^{0.63}. \quad (1)$$

BGD
7, 5047–5079, 2010

The particular value Φ=1 stands for the mean Case 1 waters conditions. If CDOM is in "excess" compared to its mean value as expected from the [Chl] value, then Φ is >1; Φ can as well be <1, when the CDOM content is below its expected average value.

The derivation of the Φ index from ocean color radiometric data is briefly recalled in what follows. It results from the simultaneous consideration of the spectral reflectance, $R(\lambda)$, at four wavelengths (λ=412,443,490 and 555 nm), and then by forming the two independent ratios, $R(412)/R(443)$ and $R(490)/R(555)$, hereafter denoted R^{412}_{443} and R^{490}_{555}. In mean case 1 waters, i.e., when Φ=1, a univocal relationship links R^{412}_{443} to R^{490}_{555}, and is represented by a unique curve within the R^{412}_{443}–R^{490}_{555} plane. In this plane, a family of similar curves is produced when Φ is given various discrete values around 1 (Fig. 2, in Morel and Gentili, 2009a). For each pixel of the SeaWiFS imagery, Φ is simply obtained by considering the two ratios R^{412}_{443} and R^{490}_{555} computed from the reflectances retrieved at this pixel, and by comparing them with the curves drawn within the R^{412}_{443}–R^{490}_{555} plane (see also discussion in Appendix A. In practice, an interpolation into a 2-D lookup table, which is numerically equivalent to the family of curves, allows the determination of the Φ index (available at ftp://oceane.obs-vlfr.fr/pub/gentili/CDM-index-Table.interpol). Once Φ has been determined, the coefficient $a_y(443)$ can be computed through Eq. (1) by using the [Chl] value determined at the same pixel via the standard algorithm (actually OC4v6 used in the last reprocessing labeled 2009.1).

As a consequence of the presence of yellow substance in varying proportions with respect to [Chl] (i.e., as a consequence of varying Φ values), the [Chl] values retrieved by using a standard univocal algorithm may be erroneous. Indeed, standard algorithms (as for instance OC4 presently used to retrieve [Chl]) implicitly suppose that the average proportions between CDOM and [Chl] are respected; in other words they imply that Φ∼1. When Φ differs from unity, the [Chl] estimate is subsequently biased (Siegel et al., 2005; Hu et al., 2006; Morel end Gentili, 2009a, their Fig. 9). An overestimation occurs when Φ>1, since the "excess" of CDOM is converted through the nominal algorithm into an increased [Chl] value; therefore the correction to be applied is a negative

BGD
7, 5047–5079, 2010

one. The converse holds true if $\Phi<1$. The corrected [Chl] values are conveniently obtained through the use of a lookup table with Φ and the initial (uncorrected) Chl value as entries, available at <ftp://oceane.obs-vlfr.fr/pub/gentili/ChlCorrected-Table.interpol>.

An additional remark is useful and deals with the appellation and meaning of the so-called quantities CDM and CDOM. As a product of the GSM method (Maritorena et al., 2002; Siegel et al., 2002), the CDM acronym, with the meaning of "colored *detrital* material", was introduced. It represents the combined absorption of colored detrital particles and of dissolved organic material. The latter component, which largely dominates the absorption process, is often referred to as CDOM (for Chromophoric *dissolved* organic matter, i.e., the matter able to pass through a membrane filter with 0.2 µm pore size). The quantity which is retrieved here and used in the present study is close to CDOM (and is referred to as such), even if does not exactly fulfill the definition (which involves filtration; see discussion in Morel and Gentili, 2009a).

3 The selected geographic zones

Six quadrangular zones were selected within the five major anticyclonic gyre systems of the three oceans (McClain et al., 2004). These zones are located to coincide with the cores of the gyres in the northern and Southern Hemispheres, and where [Chl] is minimal (see Fig. 1, and Table 1 providing the locations and limits). In such central positions within the anticyclonic circulations, the lateral advective exchanges are supposedly reduced to their minimum. The central parts were delimited through a simple statistical analysis and by progressively reducing the area under consideration to isolate the zones exhibiting the lowest, and spatially homogeneous, [Chl] values (method described in Fougnie et al., 2002). The low [Chl] values do not imply a constancy in the concentration. Actually, a clear seasonal signal occurs in four of the six selected zones (see later on), while in the two others, fluctuations in [Chl] also occur, but appear less organized.

BGD
7, 5047–5079, 2010

The South Pacific gyre is the largest subtropical anticyclonic gyre of the world ocean and its hyperoligotrophic character was already acknowledged (Claustre et al., 2008; Morel et al., 2007a). Its central zone, around Easter Island, is presently selected. Its counterpart in the Northern Hemisphere is also a wide anticyclonic system, extending from Hawaiian Islands to Mariana Islands. The preliminary study showed that the most oligotrophic waters are lying in the westernmost part of the gyre, i.e., east of Mariana Islands; this zone, actually within the so-called warm pool, was selected.

In the Atlantic ocean, the generally low level of phytoplankton in the Sargasso Sea is known for a long time (Menzel and Ryther, 1960, 1961), and regularly documented (Bermuda Atlantic Time-Series Study or "BATS" program; see e.g., Michael and Knap, 1996). The area presently selected in the southern Sargasso Sea, between 22° and 27° N, lies south of the BATS deployment, where the [Chl] level may be moderately high in winter (Garver and Siegel, 1997); this area is thus close to the study site selected by Hu et al. (2006) and presumably stable. Indeed, the mesoscale eddy activity, which may include intermittent drift of cold core rings at the latitude of Bermuda, is reduced southward, at latitudes <27° N (Steinberg et al., 2001).

The South Atlantic gyre off Brazil is similarly characterized by a low algal content with apparently a limited E–W extension probably due to the remote influence of the eutrophic Benguela system (Fig. 1). Data obtained along the Atlantic Meridional Transect (Aiken et al., 2009) have regularly confirmed the low [Chl] values in this area. Midway between Madagascar and Australia, in the South Indian ocean, the scarcely documented anticyclonic gyre is systematically seen by ocean color sensor as an oligotrophic zone, and thus was also retained for the present study.

Finally, another area situated south of the Hawaiian Islands has also been considered. Actually, this area belongs to the North Pacific subtropical gyre system, but does not exhibit the lowest [Chl] level in the North Pacific (which, as said before, was found near the Mariana Islands). This area was nevertheless considered for a comparative study, in particular because in situ data are regularly gathered nearby, at the ALOHA reference station, and at the MOBY instrumented site, devoted to satellite

BGD
7, 5047–5079, 2010

calibration/validation and optical measurements. The region presently selected, however, is more in the south, (i.e., south of 18° N). It is outside of the eddy activity field in the lee of the Hawaiian Islands (Calil and Richards, 2010), yet inside the northern branch of the North Equatorial current (Wyrtki and Kilonsky, 1984); therefore, lateral advection is likely non negligible.

At first sight (Fig. 1), the CDOM distribution in the upper layer bears a rough resemblance to the phytoplanktonic chlorophyll distribution. The modulation introduced by the Φ factor (Eq. 1) impedes a tight correlation between the two quantities; nevertheless, the selected oligotrophic areas are generally characterized by low a_y values.

4 Results

The monthly [Chl] and Φ SeaWiFS values, from January 1998 to December 2007, have been spatially averaged over each of the six zones. With these values, the corresponding CDOM absorption values, $a_y(443)$, have been straightforwardly derived via Eq. (1). These quantities are displayed in Fig. 2. Then, annual climatologies (12 months) were produced for each zone by cumulating and averaging the cycles observed during the ten years (Fig. 3). Finally, annual mean values with their standard deviations were also computed from these cycles. They are provided in Table 2, where the zones have been ranked according to increasing [Chl] values. When needed, the eight-day [Chl], Φ, and PAR composites have also been examined ("PAR" means "photosynthetically available radiation", from 400 to 700 nm).

4.1 The chlorophyll concentration

The permanent oligotrophic character is confirmed within the six selected areas. The annual mean [Chl] values are below 0.06 mg m^{-3} everywhere (Table 2) to be compared to 0.193 mg m^{-3}, the mean value for the deep global ocean (Wang et al., 2005). Yet, notable differences occur between the South Pacific gyre (Easter Island, E), which

BGD
7, 5047–5079, 2010

definitely appears to be hyperoligotrophic (mean [Chl] 0.026 mg m^{-3}), and the North Pacific gyre (near Hawaii, H), which admittedly is not located at the center of this gyre, and where the mean [Chl] value (0.059 mg m^{-3}) is the highest one. The South Atlantic (B) and Indian (I) gyres, and the Sargasso Sea (S) are in intermediate trophic positions, with annual mean [Chl] values ranging from 0.039 to 0.049 mg m^{-3}.

The temporal variability is reflected by the standard deviation (σ) around the mean annual value (Table 2). The corresponding coefficients of variation (σ/mean) range from 35% (Sargasso Sea) to 65% (Easter Island). This variability essentially results from, and roughly reflects the amplitude of the seasonal cycles (Fig. 2) in the zones where such regular seasonal patterns occur (namely in E, B, I, and S). In contrast, the seasonal variability is less organized in the North Pacific gyre (M and H), while inter-annual variations are apparent; in H, [Chl] values may intermittently be rather high (> 0.10 mg m^{-3}, see also Fig. 4).

4.2 The CDOM content

The CDOM absorption coefficient in surface waters exhibits in the six zones low annual mean values. They agree with field values in the South Pacific gyre (Bricaud et al., 2010), and qualitatively, with those at 325 nm measured by Nelson et al. (2010). The present $a_y(443)$ values range from about 0.0032 (Subtropical Pacific) to ~0.0072 m^{-1} (Sargasso Sea), to be compared with the median value for the whole ocean amounting to ~0.009 m^{-1} (Morel and Gentili, 2009a). From this point of view, the selection of the oceanic zones, which has been made on the basis of [Chl], would have remained almost unchanged if, instead, a criterion based on CDOM absorption was used (compare upper and lower panels in Fig. 1). The ordering of the zones would have been different, however. Indeed, the Φ values are either below or above 1, so that the relative [Chl]-a_y proportions vary from one area to another one. With the highest average Φ value (~1.68±0.30) in the Sargasso Sea, there is a permanent excess of CDOM

BGD
7, 5047–5079, 2010

(with respect to the average); the mean $a_y(443)$ value is about $0.0072\,m^{-1}$, versus $0.0041\,m^{-1}$, the value expected if Φ was unity.

Conversely, Φ is notably <1 near the Mariana islands, which denotes a CDOM content below the average; the mean $a_y(443)$ value found in this zone ($0.0032\,m^{-1}$) actually is the lowest one, even slightly below that found near Easter Island. The region south of Hawaii also exhibits rather low $a_y(443)$ values. In the Northern Hemisphere, the difference between the two oceans is striking; the respective positions of the CDOM and [Chl] curves for the Sargasso Sea are inverted compared to those in both zones of the northern Pacific (Figs. 2 and 3).

The diversity of the various oligotrophic domains with respect to their relative contents is also indirectly illustrated by Fig. 4a, where the eight-day mean [Chl] and contemporaneous $a_y(443)$ values are displayed. The relative proportions CDOM-to-[Chl], (i.e., the Φ index) appear to be a typical trait of each region.

4.3 The Φ index and corrected [Chl] values

In the three Pacific zones (E, M, H), this index is close to, or even below unity, while it is above 1 in the Atlantic and Indian gyres. It also exhibit a seasonal pattern (except near Hawaii) to be discussed later. The amplitude of the variations in Φ is less than it is for the other quantities, which means that CDOM and [Chl] remain partly correlated in their variations. When averaged over the six zones, the coefficient of variation (σ/mean) amounts to 48.6%, 32.6% for [Chl] and a_y, respectively, and only to 20.4% for Φ. If, as noted above, the CDOM-to-[Chl] proportions are rather site specific, they nevertheless exhibit periodic variations (Figs. 2 and 3).

As in the present study Φ is never far from 1, the corrections (in both directions) to be applied to the initial [Chl] values remain limited (Table 2), except in the Sargasso Sea and Indian Ocean, where the subtractive corrections amount to ∼15–20%. In North Pacific (M and H), there is practically no correction, as it can be seen on Fig. 4b,

BGD
7, 5047–5079, 2010

derived from Fig. 4a, and where the corrected [Chl] values are plotted versus the initial (OC4v6) [Chl] values.

4.4 Similarity and differences between the oligotrophic gyres

The [Chl] and $a_y(443)$ seasonal variations within the six zones over the 1998–2007 decade (Fig. 2, see also Fig. 3) present two kinds of patterns which can be distinguished, as follows

i) A first group includes four zones, namely the South Pacific, S-Atlantic, S-Indian gyres, and the South Sargasso Sea (E,B,I,S). In these zones the seasonal cycles are strongly printed, with (single) maxima in [Chl] and in a_y which are roughly coinciding; a factor of ~2 characterizes the amplitude (maximum-to-minimum) of these seasonal cycles for both [Chl] and CDOM. These maxima occur within the two months following the winter solstice of the corresponding hemisphere; they are roughly contemporaneous of the maximal extent of the mixed layer (Fig. 5, where the monthly average mixed layer depths are displayed for the six zones). The seasonal signals, of sinusoidal and symmetrical appearance, are very similar in the three locations of the Southern Hemisphere, with an enhanced amplitude in the Indian Ocean. Although regular, the seasonal patterns in the Sargasso Sea appear more complicated, in particular because a secondary maximum occurs at the end of September and concerns both [Chl] and a_y. The seasonal cycles of the Φ index are also regular; despite the rather parallel evolutions of a_y and [Chl], their relative proportions are not constant, but seasonally changing. A s a general rule, the Φ maximum is slightly shifted (about one month) with respect to the a_y maximum; a similar shift also affects the minima.

ii) The second group includes the two locations in the North Pacific (M and H), where the variations in [Chl] and a_y appear less organized, of lesser amplitude, and only partly correlated; the Φ and a_y cycles remain concomitant, however. Near Mariana Islands, a situation reversed with respect to those encountered in the first

BGD
7, 5047–5079, 2010

group prevails. Indeed, instead of coincident phasing, there is a half year shift between the maximum in [Chl] (July), and the maximum in a_y (January), i.e., when the pycnocline is at its deepest level (Fig. 5). South of Hawaii, the numerous [Chl] and a_y fluctuations (Fig. 2) appear somewhat erratic, perhaps as consequence of lateral advective events and of the absence of significant pycnocline motion. Nevertheless, [Chl] and a_y fluctuate more or less in phase, and the Φ index remains close to 1. The climatology (Fig. 3) tend to reveal in H and M a weak [Chl] maximum in summer (June) with a particularly low maximum-to-minimum [Chl] ratio (1.15 to 1.30), and a CDOM maximum in January (and perhaps another one in July, south of Hawaii).

It is worth noting that the presence (Sargasso Sea) or quasi-absence (Hawaii) of seasonality was already pointed out by Siegel et al. (2002), who produced and studied time series of CDM in the BATS and HOT sites. Their CDM values are slightly above the present a_y values. Actually the algorithms providing CDM and a_y differ, possibly leading to a small divergence (with CDM>a_y) as already noticed (Fig. 7c and d in Morel and Gentili, 2009a). Besides, with the intent of isolating the most oligotrophic cores, the presently selected S and H zones are both southwardly shifted compared to the BATS and HOT sites.

5 Analysis of the seasonal variations

According to the subtropical latitude of the zones under study, the winter vertical mixing, generally occurring shortly after the winter solstice (Fig. 5), is somewhat reduced in intensity. Despite its limited amplitude, the deepening of the thermocline is apparently sufficient to allow underlying waters, with their nutriments and unbleached yellow substance content, to shoal and to be exposed to solar radiation. The response in terms of chlorophyll concentration (perhaps influenced by photo-adaptation – see discussion below) is fast, so that the [Chl] and CDOM peaks associated with vertical mixing events are simultaneous. This simultaneity, even at high frequency, is supported

BGD
7, 5047–5079, 2010

by the detailed examination of the SeaWiFS data obtained at the eight-day resolution near Easter Island (Tables 1 and 2, Fig. 6a); the mixed layer depth, as derived from the data recorded in this zone by an ARGO float at a ten-day resolution (see legend), is also displayed in this Figure.

This is the typical scenario within the four zones of the first group, so that a "winter Chl maximum" regularly occurs there, in agreement with the "model 3" in Longhurst (1995). Its progressive development begins in fall, and the peaks occur in July-August in the Southern Hemisphere and in January in the Sargasso Sea; then [Chl] declines smoothly. Compared to stronger mid-latitude "spring blooms", the subtropical winter bloom appears moderate, as the ratio between the [Chl] maximum and its minimum barely reaches 2.5. The temporal evolution of the CDOM content mimics that of [Chl] with coinciding peaks and a maximum-to-minimum ratio also of about 2. Yet, the a_y – [Chl] proportions are periodically changing, as demonstrated by the Φ cycles which generally have their maximum about one month (8 to 40 days) after the [Chl] peak. This time lag could mean that the decrease in CDOM, presumably due to the photo-bleaching process, is slower than the [Chl] decline. It may also indicate that a certain amount of CDOM is locally produced by algae during their degradation. This phase lag persists during the whole summer, since Φ reaches its minimum not before October (Northern Hemishere) or March–April (Southern Hemisphere), i.e., when [Chl] has already begun to increase again. Similar observations of time lags were made by Hu et al. (2006) in a location within the Sargasso Sea (65° W–27.5° N). In passing, it is worth noting that their ag-443 values (Hu et al.'s notation), within the range 0.0035–0.009 m^{-1}, and the present $a_y(443)$ values are in excellent agreement as regards their magnitude and seasonality.

There is also another systematic feature appearing in the Φ cycles (Fig. 2): it consists of a "shoulder" occurring when [Chl] approaches its minimum around January (E,B, and I), or in June–July (Sargasso Sea, where this feature is particularly developed). Its origin, perhaps to be found in a grazing activity, remains unclear.

BGD
7, 5047–5079, 2010

For the second group which comprises M within the warm pool, and H within the North Equatorial current, the situation is very different, for the presence of strong haloclines and barrier layers impedes active convection. The supplying of nutrients and CDOM to the upper layer is somewhat limited; as a consequence, the seasonality of the [Chl] and a_y signals is partly erased, and is replaced by intermittent weak [Chl] peaks in M, or prominent peaks in H, often occurring in mid-summer and differing in intensity from year to year.

As for CDOM, the two sites have in common a weak maximum in winter (January), in coincidence with the moderate deepening of the mixed layer (Fig. 5). In H, there is a second CDOM maximum in June–July coinciding with the weak [Chl] maximum, and a second deepening of the mixed layer (Fig. 5). In M, both the CDOM content and Φ remain low all the year round in these less saline well-lit surface waters of the warm pool. In this site, a CDOM cycle is discernable along the 10 yr record (Fig. 2), with a systematic minimum from April to September, when the thermocline is at its shallower level (Fig. 5) and solar bleaching is particularly effective; the weak a_y and [Chl] maxima are in opposite phase (Fig. 3). On the contrary, south of Hawaii, the a_y fluctuations (Fig. 2) roughly parallel those of [Chl], suggesting a common cause.

6 Discussion and conclusion

With significantly differing [Chl] and CDOM content, the six zones are not identical from an optical viewpoint.

The South Pacific gyre, the world largest oceanic desert, is the area where the clearest waters were found so far (Morel et al., 2007a). The area near Mariana islands, with a slightly higher mean [Chl] content and a similar low CDOM content (see also Omori et al., 2010), is probably of exceptional clarity regardless of the season. According to the present results, no other oligotrophic systems exhibit so low pigment and yellow substance contents. In particular, the Sargasso Sea which is often considered as an archetype for oligotrophic regime, is certainly not the bluest sea. Even if the lowest

BGD
7, 5047–5079, 2010

CDOM values in the North Atlantic were observed in this zone (Nelson et al., 2007), they still are the highest ones among the six zones presently considered. Note that a similar statement was already formulated for the rather oligotrophic Mediterranean Sea, where the waters are not as blue as it could be expected from their low [Chl] level, essentially because of a relative excess of CDOM (Morel and Gentili, 2009b). For in-flight calibration or inter-comparison of ocean color space sensors over known targets, the seasonal variations here described have to be accounted for, as they affect the water reflectance in the blue and UV spectral domains. The seasonality is rather reproducible from year to year in four sites (E, B, I, and S). The site near Mariana Islands, deprived of seasonal signal, is very stable and particularly convenient for ocean color calibration. According to a recent study, the ocean's most oligotrophic waters are expanding (Polovina et al., 2008). As a possible consequence, the core of the oligotrophic gyres could perhaps become even more oligotrophic. Nevertheless, the attempt to detect such a temporal evolution over the 10-yr time series has not revealed any significant trend.

From a biochemical viewpoint, the oligotrophic regimes in the subtropical gyres are akin without being identical; in particular, the two groups defined above exhibit distinctive features. In the two North Pacific sites, the seasonal signals for both [Chl] and a_y are either erratic (in H) or featureless (in M), and there is no clear explanation to such behaviors, probably related to the permanence of a rather thin mixed layer and the absence of deep convection. In contrast, within the four sites of the first group (i.e., E, B, I, and S), repetitive seasonal signatures appear, and the concomitance of the [Chl] and CDOM temporal variations, in phase and even in relative amplitudes, is striking. This feature calls for a comment, and an attempt to find an explanation. Several scenarios are possible and three will be examined. They involve as main processes the local production of CDOM by algae, the algal photoacclimation and the reduction of the bleaching during winter, and finally, the vertical flux of nutrients and CDOM associated with the winter convection.

BGD
7, 5047–5079, 2010

To explain the simultaneous raising in [Chl] and CDOM, it is tempting to imagine that the dissolved colored matter is straightforwardly produced by the algal population, either directly (cell lysis, excretion), or indirectly (through prompt "sloppy" feeding and heterotrophic activity). The CDOM content would thus go along with the phytoplanktonic development. Such an explanation implies that the production of CDOM by algae is an extremely fast process. Actually, this hypothesis was adopted by Hu et al. (2006). These authors also based their interpretation on the small time lag (by about two weeks) they have observed between the [Chl] maximum and the development of a CDOM maximum. The results obtained here, even at the eight-day resolution, do not show that such a lag is systematic nor is a significant feature; at this resolution, the highest a_y values are closely associated with the highest [Chl] values (Fig. 2; see also Fig. 6a). Actually, the coincidence between the (Chl) and the a_y peaks, which seems to be shared by the subtropical areas, is not, by far, a general rule; a previous result, summarized as follows, has to be considered. In temperate latitude, namely in the Western Mediterranean Sea, as well as in the entire zonal 30°–45° N belt, (Morel and Gentili, 2009b), it has been observed that the onset of the CDOM increase occurs when the autumnal process of the thermocline erosion begins, and the CDOM maximum (in January), precedes the vernal bloom (in March). For a detailed confirmation of this process, an area was selected in the transition zone at latitudes between 34° and 40° N, off Gibraltar and outside of the Portuguese upwelling (Fig. 1, Table 1). The corresponding time series at eight-day resolution, displayed in Fig. 6b, clearly shows that the maximum in CDOM, which is in phase with the deepest convection (see Fig. 5), precedes the vernal Chl-bloom by about 6–8 weeks. Such a delay between the CDOM peak and the [Chl] peak is obviously not in favor of a fast production of CDOM by the blooming algal standing stock.

A second hypothesis which can also be considered is related to the diminishing solar irradiation during winter. At the subtropical latitudes, the daily photosynthetically available radiation at the surface, PAR(0), is roughly reduced by a factor 2 in winter, compared to its value in summer; an example for the zone in the vicinity of Easter Island

BGD
7, 5047–5079, 2010

is provided by Fig. 7a . This reduction is not considerable, but if it is assumed that the phytoplanktonic cells are passively transported by turbulence within the entire extended mixed layer, the radiant energy they receive *on average*, denoted $\overline{\text{PAR}}$, is much less (see Appendix B for its computation). Actually, the $\overline{\text{PAR}}$ value in winter is reduced by a factor of about 10 compared to its value in summer, as a consequence of the deepening of the mixed layer (Fig. 6c, and Appendix). This reduction in radiant energy may have two consequences, on the [Chl] value, and on the CDOM value. Indeed, it cannot be excluded that a photoacclimation process intervenes and results in an increase in chlorophyll cellular content and thus in [Chl], whereas the algal biomass would stay essentially unchanged. According to this scenario, the progressive [Chl] increase during winter as detected by ocean color imagery would be an effect of photoacclimation. For the same reason, the solar bleaching which affects the CDOM becomes less efficient when exerted upon the entire mixed layer. Therefore unbleached CDOM brought upward by the progressive vertical mixing is able to persist without major damage during the winter period.

The third scenario is simply based on the vertical mixing, which begins in fall when the heat budget becomes negative, and progressively brings upward both unbleached CDOM and nutrients. The CDOM pool is progressively built up. With the nutrient supply phytoplankton commence to develop, but only slowly. At moderate (or high) latitudes, according to the classical scheme, the light limitation and a lack of stratification prevent algae from growing actively, so that the bloom itself is delayed until spring, when light and stability are sufficient. It is postulated here that these limitations (the light level, especially) are less stringent in subtropical zones (the Longhurst's "model 3"), so that the time lag between the CDOM and [Chl] maxima vanishes. In this scheme, the coincidence of the two maxima would not be the straight expression of a causal relationship (i.e., instantaneous CDOM production by developing algae), but the consequence of the same cause (i.e., the convective mixing). This conjecture is supported by the observations of the opposite situation: in absence of efficient vertical mixing (in the site M, especially), [Chl] and the CDOM content stay permanently at their lower

BGD
7, 5047–5079, 2010

level (Table 2 and Fig. 4). Such an explanation involving as the main factor the vertical transport of CDOM is congruent with previous observations (Nelson et al., 1998) showing that CDOM is essentially produced in the subthermocline layer by local heterotrophic processes leading to a remineralization of sinking particulate organic matter. Recent findings (Swan et al., 2009; Nelson et al., 2010) show that this oxidative process in deep waters is reflected by the correlation observed between CDOM and AOU, the apparent oxygen utilization. Less deep, within the subthermocline layer, the production of colored dissolved material is probably related to the average photosynthetic production within the upper well-lit layer which governs the downward vertical flux of materials. Such a link could explain the differences between the sites in terms of average CDOM level (Note that this explanation fails in the case of the Sargasso Sea, since [Chl] in the surface layer is low while CDOM is relatively high, as in other parts of the North Atlantic).

The complex interactions regulating the upper layer CDOM concentration were already hypothesized by Siegel et al. (2002, their Fig. 6 for instance). Nevertheless the respective weight of the various processes (local production versus vertical transport, accumulation versus photo-degradation) is largely unknown. The three scenarios above have been independently described for the sake of clarity. It is not only plausible but highly probable that they can coexist. Detailed vertical profiles of both quantities, [Chl] and CDOM, as well as of nutrients and physical/optical conditions, as soon available with profilers (such as Bio-Argo profilers), are needed to get a better understanding of the interwoven processes at play and of their respective contribution.

Appendix A

Sensitivity study to the slope value of the CDOM spectral absorption

A family of curves (numerically a 2-D lookup table) representing the relationship between the ratios R_{443}^{412} and R_{555}^{490} within the R_{443}^{412}–R_{555}^{490} plane is produced when Φ is

BGD
7, 5047–5079, 2010

given various discrete values around 1; these curves form a "grid" which is represented in Fig. 2b (in Morel and Gentili, 2009a). These computations are made by using the semi-analytical reflectance model described in Morel and Maritorena (2001). When Φ differs from unity, it is necessary to adopt a spectral dependency for the CDOM absorption, which is, as usual, expressed according to

$$a_y(\lambda) = a_y(\lambda_0)\exp[-S(\lambda-\lambda_0)], \quad \text{(A1)}$$

where λ_0 is a reference wavelength, and S (nm^{-1}) is the exponential decay within the spectral range considered (412–555 nm). The average slope S presently adopted is $0.018\,\mathrm{nm}^{-1}$. A sensitivity study with respect to this S value is based on the grids which are obtained when S is given other plausible values. The same couples of ratios R^{412}_{443} and R^{490}_{555} introduced into these differing grids provide differing Φ values. Actually they do not differ much: when S is changed from 0.018 to $0.022\,\mathrm{nm}^{-1}$, Φ is diminished by, at the most, 10% for Φ between 1 and 2; or, conversely, it is increased by, at the most, 10% when Φ is between 1 and 0.5. These figures are to be inverted for a S change from 0.018 to $0.014\,\mathrm{nm}^{-1}$. In the present study, with values never far from unity, the effect of the hypothesis made for S is largely negligible. The discrepancies on the resulting Φ values become more important (±25%) when Φ strongly deviates from 1 and approaches values like 0.2 or 5. These effect are independent of the [Chl] values.

Appendix B

Average PAR value within the mixed layer

The average value of the Photosynthetically Available Radiation, denoted $\overline{\mathrm{PAR}}$ within a layer is the average value of the integral of the PAR(z) profile over the layer in question; here the layer considered is the mixed layer of thickness Z_{mld}, so that

BGD
7, 5047–5079, 2010

$$\overline{\mathrm{PAR}}=(1/Z_{\mathrm{mld}})\mathrm{PAR}(0)\int_0^{Z_{\mathrm{mld}}}\exp(-K_{\mathrm{PAR}}Z)\mathrm{d}Z\,,$$

$$\overline{\mathrm{PAR}}/\mathrm{PAR}(0)=(1/K_{\mathrm{PAR}}Z_{\mathrm{mld}})[1-\exp(-K_{\mathrm{PAR}}Z_{\mathrm{mld}})]\,,$$

where PAR(0) is the PAR value just below surface, K_{PAR} is the downward attenuation coefficient for PAR. The PAR(0) used here is the daily irradiation (as Einstein m^{-2}) derived from the SeaWiFS data; K_{PAR} can be derived from the $K_{\mathrm{d}}(490)$ the downward attenuation coefficient for the irradiance at 490 nm, or as well from [Chl] (see Eq. 8 and 9′ in Morel et al., 2007). Such a computation is only an approximation (e.g., K_{PAR} considered as constant along the depth and along the day), but it suffices for what it is intended for. For typical clear waters, with $K_{\mathrm{PAR}}\sim 0.05\,\mathrm{m}^{-1}$, the ratio $\overline{\mathrm{PAR}}/\mathrm{PAR}(0)$ is 0.2 or 0.63 when $Z_{\mathrm{mld}}=100$ or 20 m, respectively. The stronger reduction (by the factor 0.2) applies in winter, when Z_{mld} is maximal and PAR(0) minimal.

Acknowledgements. The authors would like to thank the NASA SeaWiFS project at the Goddard Space Flight Center for maintenance, processing , and efficient distribution of the SeaWiFS data products. This paper represents a contribution to the remOcean project (remotely sensed biogeochemical cycles in the Ocean), funded by the European Research Council.

The publication of this article is financed by CNRS-INSU.

BGD
7, 5047–5079, 2010

References

Aiken, J., Pradhan, Y., Barlow, R., Lavender, S., Poulton, A., Holligan, P. M., and Hardman-Mountford, N.: Phytoplankton pigments and functional types in the Atlantic Ocean: a decadal assessment, 1995–2005, Deep-Sea Res. Pt. II, 56, 899–917, 2009.

Antoine, D., André, J.-M., and Morel, A.: Oceanic primary production, 2. Estimation at global scale from satellite (coastal zone color scanner) chlorophyll, Global Biogeochem. Cy., 10, 57–69, 1996.

Bricaud, A., Babin, M., Claustre, H., Ras, J., and Tièche, F.: Light absorption properties and absorption budget of South East Pacific waters, J. Geophys. Res., in press, 2010.

Calil, P. H. R. and Richards, K. J.: Transient upwelling hot spots in the oligotrophic North Pacific, J. Geophys. Res., 115, C02003, doi:10.1029/2009JC005360, 2010.

Claustre, H. and Maritorena, S.: The many shades of ocean blue, Science, 302, 1514–1515, 2003.

Claustre, H., Sciandra, A., and Vaulot, D.: Introduction to the special section bio-optical and biogeochemical conditions in the South East Pacific in late 2004: the BIOSOPE program, Biogeosciences, 5, 679–691, doi:10.5194/bg-5-679-2008, 2008.

de Boyer Montegut, C., Madec, G., Fisher, A. S., Lazar, A., and Iudicone, D.: Mixed layer depth over the global ocean: an examination of profile data and a profile-based climatology, J. Geophys. Res., 109, C12003, doi:10.1029/2004JC002378, 2004.

Fougnie, B., Henry, P., Morel, A., Antoine, D., and Montagner, F.: Identification and characterization of stable homogeneous oceanic zones: climatology and impact on in-flight calibration of space sensor over Rayleigh scattering, Ocean Optics XVI, Santa Fe, NM, 18–22 November, 2002.

Garver, S. A. and Siegel, D. A.: Inherent optical property inversion of ocean color spectra and its biogeochemical interpretation, 1. Time series from the Sargasso Sea, J. Geophys. Res., 102, 18607–18625, 1997.

Hu, C., Lee, Z., Muller-Karger, F. E., Carder, K. L., and Walsh, J. J.: Ocean color reveals phase shift between marine plants and yellow substance, IEEE T. Geosci. Remote, 3, 262–266, 2006.

Longhurst, A.: Seasonal cycles of pelagic production and consumption, Prog. Oceanogr., 36, 77–167, 1995.

BGD
7, 5047–5079, 2010

Maritorena, S., Siegel, D. A., and Peterson, A.: Optimization of a semi-analytical ocean color model for global applications, Appl. Optics, 41, 2705–2714, 2002.
McClain, C. R., Signorini, S. R., and Christian, J. R.: Subtropical gyre variability observed by ocean-color satellites, Deep-Sea Res. Pt. II, 51, 281–301, 2004.
Menzel, D. W. and Ryther, J. H.: The annual cycle of primary production in the Sargasso Sea off Bermuda, Deep-Sea Res., 6, 115–128, 1960.
Menzel, D. W. and Ryther, J. H.: Annual variations in primary production of the Sargasso Sea off Bermuda, Deep-Sea Res., 7, 282–288, 1961.
Michaels, A. F. and Knap, A. H.: Overview of the US JGOFS BATS and hydrostation S program, Deep-Sea Res., 43, 157–198, 1996.
Morel, A. and Maritorena, S.: Bio-optical properties of oceanic waters: a reappraisal, J. Geophys. Res.-Oceans, 106, 7163–7180, 2001.
Morel, A.: Are the empirical laws describing the bio-optical properties of Case 1 waters consistent and internally compatible?, J. Geophys. Res., 114, C01015, doi:10.1029/2008JC004803, 2009.
Morel, A., Gentili, B., Claustre, H., Babin, M., Bricaud, A., Ras, J., and Tièche, F.: Optical properties of the "clearest" natural waters, Limnol. Oceanogr., 52, 217–229, 2007a.
Morel, A., Claustre, H., Antoine, D., and Gentili, B.: Natural variability of bio-optical properties in Case 1 waters: attenuation and reflectance within the visible and near-UV spectral domains, as observed in South Pacific and Mediterranean waters, Biogeosciences, 4, 913–925, doi:10.5194/bg-4-913-2007, 2007.
Morel, A. and Gentili, B.: A simple band ratio technique to quantify the colored dissolved and detrital organic material from ocean color remotely sensed data, Remote Sens. Environ., 113, 998–1011, 2009a.
Morel, A. and Gentili, B.: The dissolved yellow substance and the shades of blue in the Mediterranean Sea, Biogeosciences, 6, 2625–2636, doi:10.5194/bg-6-2625-2009, 2009.
Nelson, N. B., Siegel, D. A., Carlson, C. A., Swan, C., Smethie Jr., W. M., and Khatiwala, S.: Hydrography of chromophoric dissolved organic matter in the North Atlantic, Deep-Sea Res. Pt. I, 54, 710–731, 2007.
Nelson, N. B., Siegel, D. A., Carlson, C. A., and Swan, C.: Tracing global biogeochemical cycles and meridional overturning circulation using chromophoric dissolved organic matter, Geophys. Res. Lett., 37, L03610, doi:10.1029/2009GL04325, 2010.

BGD
7, 5047–5079, 2010

Omori, Y., Hama, T., Ishii, M., and Saito, S.: Relationship between the seasonal change in fluorescent dissolved organic matter and mixed layer depth in the subtropical western North Pacific, J. Geophys. Res., 115, C06001, doi:10.1029/2009JC005526, 2010.
Polovina, J. J., Howell, E. A., and Abecassis, M.: Ocean's least productive waters are expanding, Geophys. Res. Lett., 35, LO3518, doi:10.1029/2007GL031745, 2008.
Ras, J., Claustre, H., and Uitz, J.: Spatial variability of phytoplankton pigment distributions in the Subtropical South Pacific Ocean: comparison between in situ and predicted data, Biogeosciences, 5, 353–369, doi:10.5194/bg-5-353-2008, 2008.
Steinberg, D. K., Carlson, C. A., Bates, N. R., Johnson, R. J., Michaels, A. F., and Knap, A. H.: Overview of the US JGOFS Bermuda Atlantic Time-series Study (BATS): a decade-scale look at ocean biology and biogeochemistry, Deep-Sea Res. Pt. II, 48, 1405–1447, 2001.
Siegel, D. A., Maritorena, S., Nelson, N. B., Hansell, D. A., and Lorenzi-Kaiser, M.: Global distribution and dynamics of colored dissolved and detrital organic materials, J. Geophys. Res., 107(C12), 3228, doi:10.1029/2001JC000965, 2002.
Siegel, D. A., Maritorena, S., Nelson, N. B., and Behrenfeld, M. J.: Independence and interdependencies among global ocean color properties: Re-assessing the bio-optical assumption, J. Geophys. Res., 110, C07011, doi:10.1029/2004JC002527, 2005a.
Siegel, D. A., Maritorena, S., Nelson, N. B., Behrenfeld, M. J., and McClain, C. R.: Colored dissolved organic matter and its influence on the satellite-based charaterization of the ocean biosphere, Geophys. Res. Lett., 32, L20605, doi:10.1029/2005GL024310, 2005b.
Swan, C. M., Siegel, D. A., Nelson, N. B., Carlson, C. A., and Nasir, E.: Biogeochemical and hydrographic controls on chromophoric dissolved organic matter distribution in the Pacific Ocean, Deep-Sea Res. Pt. I, 56, 2175–2192, 2009.
Wang, M., Knobelspiesse, K. D., and McClain, C. R.: Study of the Sea-Viewing Wide Field-of-view Sensor (SeaWiFS) aerosol optical property data over ocean in combination with the ocean color products, J. Geophys. Res., 110, D10S06, doi:10.1029/2004JD004950, 2005.
Wyrtki, K. and Kilonsky, B.: Mean water and current structure during the Hawaii-to-Tahiti shuttle experiment, J. Phys. Oceanogr., 14, 242–254, 1984.
Yamashita, Y. and Tanoue, E.: Basin scale distribution of chromophoric dissolved organic matter in the Pacific Ocean, Limnol. Oceanogr., 54, 598–609, 2009.

BGD
7, 5047–5079, 2010

Table 1. Geographical information for the six oligotrophic zones selected for the present study; in addition, a mesotrophic site off Portugal, used for comparison (see text), as well as a sub-zone near Easter Island, where an ARGO float has been deployed, are also included.

Location	Notation	Longitude		Latitude		Surface (10^6 km^2)
Easter Island zone	E	−125.0	−100.0	−30.0	−20.0	2.794
Mariana Islands zone	M	150.0	165.9	10.0	20.0	1.787
Brasilian Atlantic gyre	B	−32.0	−25.9	−22.5	−12.5	0.823
South-Sargasso Sea	S	−70.0	−45.0	22.0	27.0	1.404
South Indian gyre	I	70.0	90.0	−30.0	−21.0	2.004
Hawaii Islands zone	H	−170.0	−150.9	10.0	18.0	1.916
Atlantic off Portugal	P	−25.0	−15.0	34.0	40.0	0.591
Argo float (E)	f	−115.0	−101.0	−29.0	−24.0	0.773

BGD
7, 5047–5079, 2010

Table 2. In reference to Table 1, annual mean values and standard deviations of the quantities [Chl] ($mg\,m^{-3}$), Φ (dimensionless), and a_y (m^{-1}), for each zone including P (Portugal) and f (ARGO float).

	Chl		corr. Chl		ϕ		a_y	
	mean	st.dev.	mean	st.dev.	mean	st.dev.	mean	st.dev.
E	0.026	0.017	0.027	0.016	1.090	0.254	0.0033	0.0015
M	0.034	0.019	0.037	0.020	0.898	0.193	0.0032	0.0009
B	0.039	0.015	0.036	0.014	1.258	0.232	0.0048	0.0015
S	0.046	0.016	0.038	0.014	1.683	0.298	0.0072	0.0018
I	0.049	0.023	0.043	0.020	1.459	0.312	0.0065	0.0024
H	0.059	0.029	0.060	0.031	1.010	0.203	0.0049	0.0014
P	0.166	0.132	0.122	0.112	2.133	0.848	0.0200	0.0128
f	0.024	0.020	0.029	0.019	1.137	0.337	0.0037	0.0019

BGD
7, 5047–5079, 2010

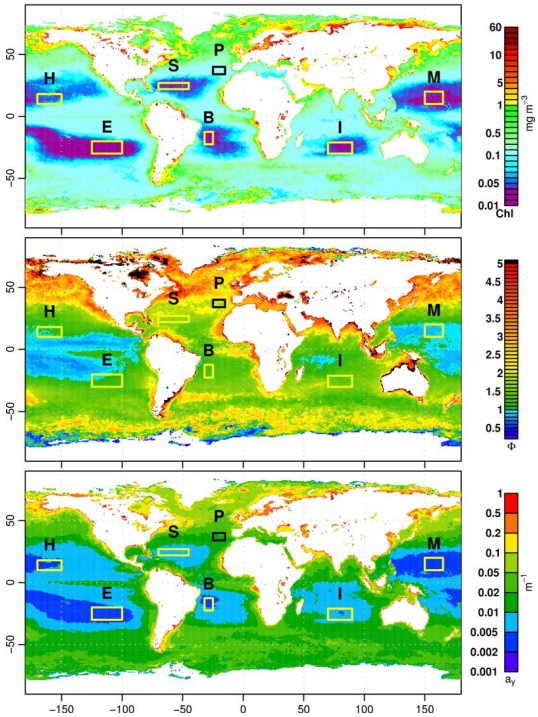

Fig. 1. Annual composite (year 2006) of SeaWiFS data for the global ocean. Upper panel: chlorophyll concentration, [Chl] (mg m^{-3}); middle panel: chromophoric dissolved matter index, Φ (dimensionless). Both these quantities are provided and distributed by NASA. Lower panel: map of the absorption coefficient at 443 nm, a_y (m^{-1}) of the chromophoric dissolved matter, CDOM, computed from [Chl] and Φ via Eq. (1). Each panel has its own color scale. The (yellow) boxes superimposed on the maps show the oligotrophic zones selected for the present study (see also Table 1 for the exact locations and meaning of the identifiers). The black box in a mesotrophic zone off Portugal (P) is selected for a comparison (see text).

BGD
7, 5047–5079, 2010

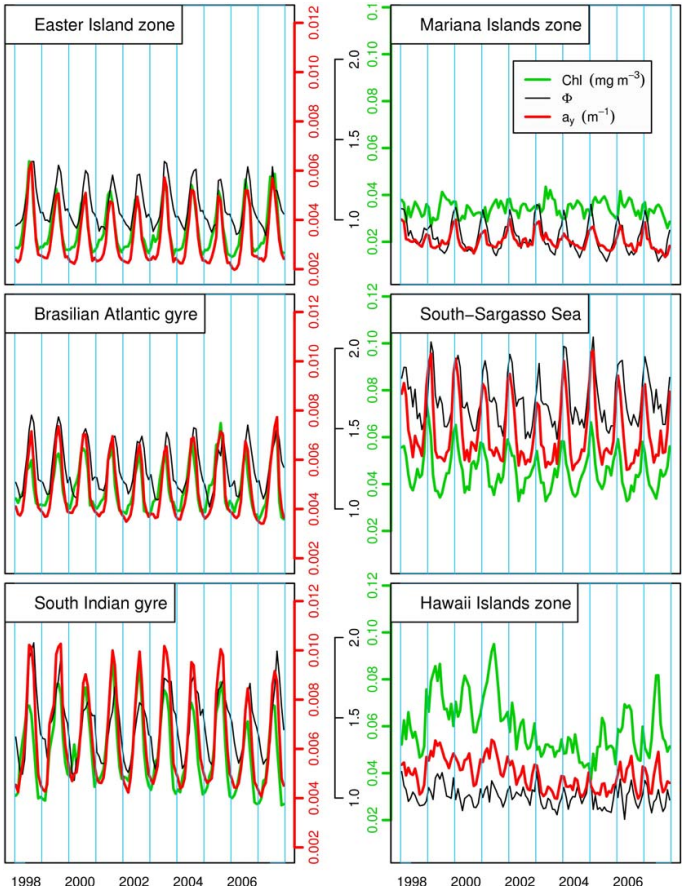

Fig. 2. Time series (1998–2007) of the three parameters, [Chl], $a_y(443)$, and Φ, as established from the monthly composites and by averaging the values of all pixels over each of the six selected zones (identifiers as in Table 1); to facilitate the comparisons, the scales are identical for the six panels.

BGD
7, 5047–5079, 2010

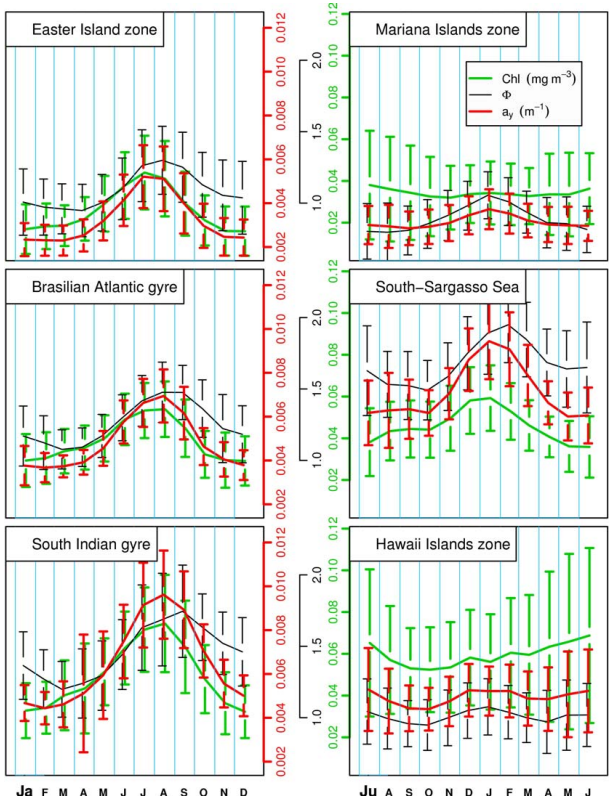

Fig. 3. Climatological annual cycles (temporal resolution: one month) within each zone of the three parameters, [Chl], Φ, and $a_y(443)$, which are obtained by averaging over 10 years the time series displayed in Fig. 2. Same symbols, colors, units, and scales as in Fig. 2; the vertical bars correspond to ±1 standard deviation. For the left hand column (sites in the Southern Hemisphere) the year starts with January; for the right hand column (Northern Hemisphere) the year starts with July; by this way, the winter solstice is in the middle of the figures, whatever the hemisphere.

BGD
7, 5047–5079, 2010

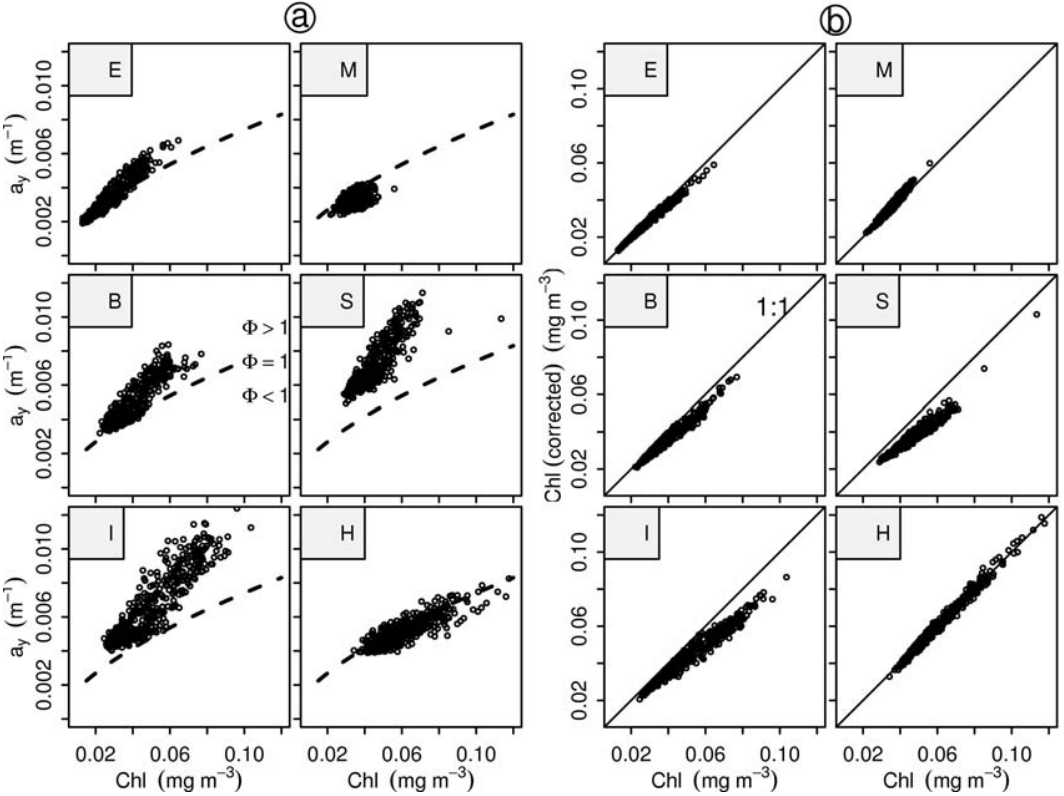

Fig. 4. **(a)**: By using the eight-day composites for each zone, spatially averaged quantities [Chl] (derived via OC4v6 algorithm), and $a_y(443)$ (derived via Eq. 1); **(b)**: corrected [Chl] versus nominal [Chl] for each zone, as in (a).

BGD
7, 5047–5079, 2010

Similarities and differences in terms of chlorophyll and yellow substance

A. Morel et al.

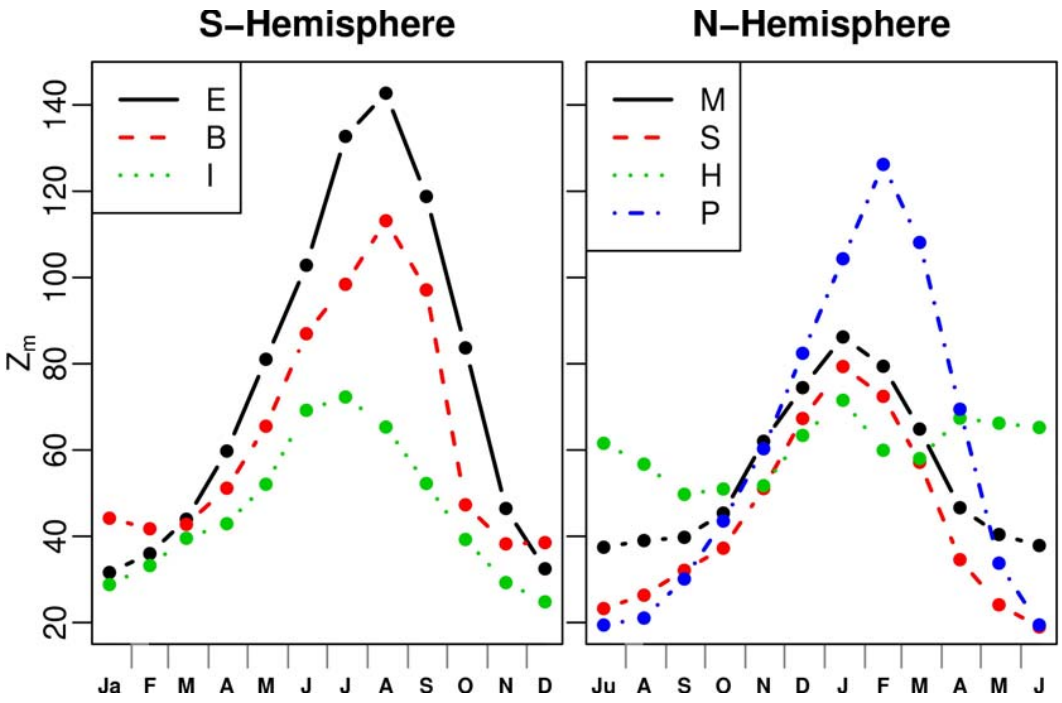

Fig. 5. Monthly values of the depth of the mixed layer (MLD) extracted from the climatology published by de Boyer Montegut et al. (2004), when the variable density criterion is used (the DReqDT-0.2 product); the MLD values which are displayed are obtained by averaging the MLD data (2° by 2° grid) over each box shown in Fig. 1. As in Fig. 3, the month scale begins with January, for the Southern Hemisphere (left panel); and in July for the Northern Hemisphere (right panel). Note that the site P (off Portugal) is not in an oligotrophic regime (see text) but is represented.

BGD
7, 5047–5079, 2010

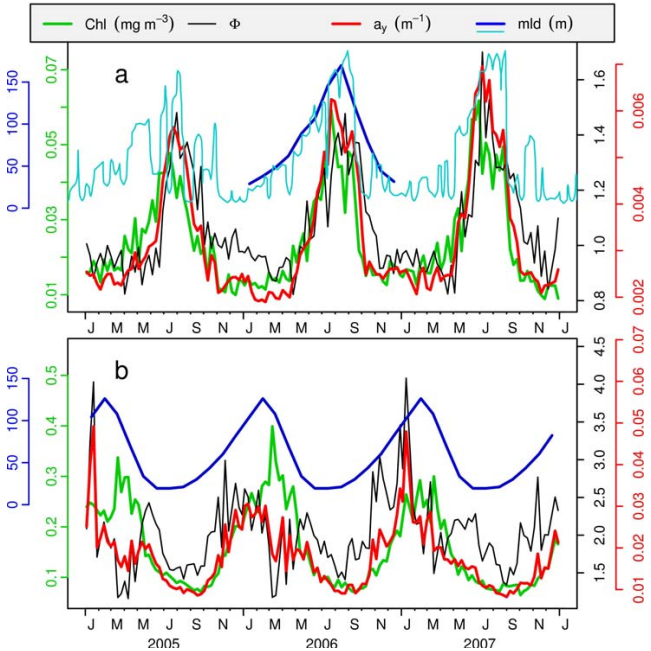

Fig. 6. (a): The three parameters, [Chl], $a_y(443)$, and Φ, are plotted with the same symbols and scales as in Fig. 2, but they are computed from the 8-day SeaWiFS L3 composites, and for a sub-zone (109°–115° W, 24°–29° S) inside the E zone, where an ARGO float (WMO 3000302) was deployed and has provided data at the 10-day frequency during the years 2005–2007. The depth of the mixed layer (Z_{mld}) was computed from the data recorded by this float, and by using a density criterion ($\Delta\sigma$=0.03); the corresponding results are shown as the (thin) blue curve. The thick blue curve represents the MLD computed for the same zone from the climatology (de Boyer Montegut et al., 2004). **(b)**: For the same years, [Chl], $a_y(443)$, and Φ are plotted also at 8-day resolution, for the zone P (off Portugal, see Tables 1 and 2). Note the change of scales between (a) and (b) (see also Table 2). The blue (thick) curve represents the climatological MLD for the P zone (from data in de Boyer Montegut et al., 2004).

BGD
7, 5047–5079, 2010

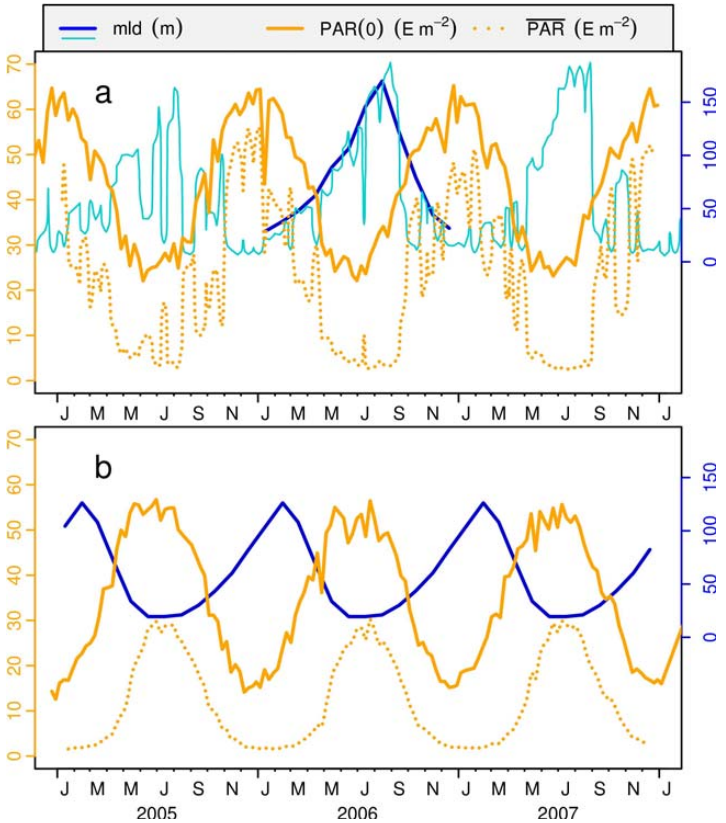

Fig. 7. The panels **(a)** and **(b)** are for the same zones as represented in Fig. 6a and b, and the depths of the mixed layer are reproduced from these panels. In addition are displayed the surface daily PAR(0) values provided by NASA and averaged over the zones in question (the solid lines), and $\overline{PAR}$, the mean values computed for the mixed layer (the dotted lines; see Appendix B). Note that the scales are the same in both panels.

BGD
7, 5047–5079, 2010